medRxiv preprint doi: https://doi.org/10.1101/2021.05.03.21256161; this version posted May 4, 2021. The copyright holder for this preprint (which was not certified by peer review) is the author/funder, who has granted medRxiv a license to display the preprint in perpetuity. It is made available under a CC-BY-NC 4.0 International license .

Validating atlas-based lesion disconnectomics in multiple sclerosis: a retrospective multi-centric study

Veronica Ravano[1,2,3], Michaela Andelova[4], Mário João Fartaria[1,2,3], Mazen Fouad A-Wali Mahdi[1], Bénédicte Maréchal[1,2,3], Reto Meuli[2], Tomas Uher[4], Jan Krasensky[5], Manuela Vaneckova[5], Dana Horakova[4], Tobias Kober[1,2,3] and Jonas Richiardi[2]

[1]Advanced Clinical Imaging Technology, Siemens Healthcare AG, Lausanne, Switzerland

[2]Department of Radiology, Lausanne University Hospital and University of Lausanne, Lausanne, Switzerland

[3]LTS5, École Polytechnique Fédérale de Lausanne (EPFL), Lausanne, Switzerland

[4]Department of Neurology and Center of Clinical Neuroscience, First Faculty of Medicine, Charles University and General University Hospital in Prague, Prague, Czech Republic

[5]MR unit, Department of Radiology, First Faculty of Medicine, Charles University and General University Hospital in Prague, Prague, Czech Republic

Corresponding author: Veronica Ravano, Advanced Clinical Imaging Technology, Siemens Healthineers, Innovation Park EPFL-QI-E,CH-1015 Lausanne, Switzerland veronica.ravano@epfl.ch

Abstract

The translational potential of MR-based connectivity modelling is limited by the need for advanced diffusion imaging, which is not part of clinical protocols for many diseases. In addition, where diffusion data is available, brain connectivity analyses rely on tractography algorithms which imply two major limitations. First, tracking algorithms are known to be sensitive to the presence of white matter lesions and therefore leading to interpretation pitfalls and poor inter-subject comparability in clinical applications such as multiple sclerosis. Second, tractography quality is highly dependent on the acquisition parameters of diffusion sequences, leading to a trade-off between acquisition time and tractography precision.

Here, we propose an atlas-based approach to study the interplay between structural disconnectivity and lesions without requiring individual diffusion imaging. In a multi-centric setting involving three distinct multiple sclerosis datasets (containing both 1.5T and 3T data), we compare our atlas-based structural disconnectome computation pipeline to disconnectomes extracted from individual tractography and explore its clinical utility for reducing the gap between radiological findings and clinical symptoms in multiple sclerosis. Results using topological graph properties showed that overall, our atlas-based disconnectomes were suitable approximations of individual disconnectomes from diffusion imaging. Small-worldness was found to decrease for larger total lesion volumes thereby suggesting a loss of efficiency in brain connectivity of MS patients. A graph embedding technique followed by dimensionality reduction found a topological organization that mirrored disability. Finally, the global efficiency of the created brain graph, combined with total lesion volume, allowed to stratify patients into subgroups with different clinical scores in all three cohorts.

NOTE: This preprint reports new research that has not been certified by peer review and should not be used to guide clinical practice.

medRxiv preprint doi: https://doi.org/10.1101/2021.05.03.21256161; this version posted May 4, 2021. The copyright holder for this preprint
(which was not certified by peer review) is the author/funder, who has granted medRxiv a license to display the preprint in perpetuity.
It is made available under a CC-BY-NC 4.0 International license .

1. Introduction

Connectivity is a powerful lens through which brain function and dysfunction can be examined. The increased availability and quality of non-invasive structural connectivity imaging using diffusion data, coupled with methodological advances, has triggered the emergence of subfields at the intersection of neuroscience and network science. In network neuroscience (Bassett and Sporns, 2017), graphs are used to model connections between brain regions, enabling an arsenal of mathematical methods which facilitate systems-level thinking and thus new ways of investigating the organization of the brain. Brain graphs are typically characterized by a set of nodes (or vertices) and a set of edges, connecting pairs of nodes (Bullmore and Bassett, 2011; Richiardi et al., 2013; Sporns et al., 2005). For the study of structural connectivity, nodes are usually defined using a brain parcellation, so that each brain area can be represented by one node, whereas edges reflect the estimated number of axonal projections connecting the corresponding brain regions. By means of graph theory, topological features can be extracted from brain networks to characterize either the overall architecture of the graph or its local properties (Bassett and Sporns, 2017; Bullmore and Sporns, 2009; Hagmann et al., 2008; Sporns et al., 2005). Typically, brain graphs are characterized by high clustering and low shortest path length, therefore leading to a so-called small-world organization (Telesford et al., 2011; Watts and Strogatz, 1998). Together with small-worldness, other topological features such as global efficiency can be computed to estimate how efficiently the information is propagated across the graph nodes: the lower the number of hops between nodes, the greater the efficiency.

Compared to raw MR images, meso- and macro-scale representations such as brain graphs have the advantage to allow better intra- and inter-subject comparability, at the expense of a loss of fine detail.

During the last decade, the study of structural connectomes, estimated from diffusion imaging with tractography, has provided a better and more extensive understanding of several neurological and psychiatric diseases. The ‘disconnectome’ approach combines the study of lesion location with structural connectomics to investigate the impact of resulting disconnections (Catani et al., 2012; Foulon et al., 2018; Fox, 2018). Where disruption of brain connectivity is found to affect higher functions, the condition can be described as a “disconnection syndrome” (Carrera and Tononi, 2014; Catani and Ffytche, 2005). Further, previous studies on the clinical impact of lesion location either in voxel-based (so called “lesion-symptom mapping” (Bates et al., 2003)) or within predefined brain networks (“lesion network mapping” (Fox, 2018)) provided a better understanding of brain functions and related diseases.

Recently, repeated findings have led multiple sclerosis (MS) to be considered a disconnection syndrome (Rocca et al., 2015). Brain damage in MS involves the transection of white matter tracts by lesions, creating a disconnection syndrome which is associated with a specific clinical phenotype (Llufriu et al., 2017). Ongoing demyelination in lesions might lead to remote axonal damage by both antero- and retrograde degeneration (“dying back“ and Wallerian degeneration (Dziedzic et al., 2010; Lucchinetti et al., 2000)). Axonal loss has been identified as the major determinant of irreversible neurological disability in MS patients (Hayes and Ntambi, 2020). An accelerated rate of brain atrophy in MS patients, together with disruption of nerve signals in the central nervous system, can cause multiple symptoms that vary widely from one patient to another. In particular, connectivity studies have shown that the overall

medRxiv preprint doi: https://doi.org/10.1101/2021.05.03.21256161; this version posted May 4, 2021. The copyright holder for this preprint
(which was not certified by peer review) is the author/funder, who has granted medRxiv a license to display the preprint in perpetuity.
It is made available under a CC-BY-NC 4.0 International license .

efficiency of functional connectomes is affected by the disease (Yaou et al., 2017) (Rocca et al., 2016)(Fleischer et al., 2019) and that small-worldness seems to dissipate with increasing lesion load (Faivre et al., 2016).

During MR examination of MS patients, radiologists typically evaluate the lesion load of their patients by counting the number of T2 hyperintense white matter lesions, but the correlation with disability is generally poor, leading to the so-called clinico-radiological paradox (Barkhof, 2002). Previous studies have shown that including lesion location improves the correlation with clinical disability (estimated using the Expanded Disability Status Scale, EDSS) (Charil et al., 2003; Vellinga et al., 2009) compared to mere lesion load. Work on topological features of structural connectomes investigated with diffusion tensor tractography (Shu et al., 2011) showed a decreased graph efficiency correlated with EDSS, disease duration and total WM lesion loads, therefore showing the potential of such new quantitative features to help narrowing this clinico-radiological gap.

Tractography is a powerful tool to model and quantify structural connectivity between brain areas based on diffusion imaging. However, although proven to be in good accordance with ex-vivo histological experiments (Buckner et al., 2011; Donahue et al., 2016) diffusion imaging and tractography methods suffer from several pitfalls. Notably, the generation of the tractography results is a model-based procedure: the diffusion signal strength and the derived tracking algorithm outcome are highly dependent not only on physiological factors and on the way axons lay in a given voxel, but also on the image reconstruction methods and acquisition parameters chosen. The quantitative interpretability of the results is therefore highly dependent on model assumptions (Jones et al., 2013) and renders inter-subjects comparisons more difficult and less reliable. Moreover, technical and time constraints arise when it comes to using tractography in clinical practice. Tracking algorithms are highly sensitive to two major time-consuming acquisition variables: spatial resolution and q-space coverage (Calabrese et al., 2014). As acquisition time is a critical limitation in clinical protocols, diffusion imaging sequences fulfilling these high standards are rarely acquired. Another possible technical limitation is the impact of white matter lesions on diffusion properties (Tievsky et al., 1999) that can in turn interfere with the tracking algorithm. Notably, abnormally low fractional anisotropy in voxels within white matter lesions can cause the termination of the tracking algorithm or cause a deviation of streamlines bundles in proximity of lesions (Ciccarelli et al., 2008), although steady progress is being made to mitigate these detrimental effects (Lin et al., 2005; Lipp et al., 2020; Pawlitzki et al., 2017; Reich et al., 2007).

To overcome these limitations, previous studies proposed to model individual structural brain disconnectivity without requiring diffusion imaging (Griffis et al., 2020; Ravano et al., 2020, 2019). Structural connectivity is approximated using the HCP842 atlas (Yeh et al., 2018), a population-averaged tractography atlas built using 842 healthy controls of the Human Connectome Project (Van Essen et al., 2012). Similarly to what was proposed by (Griffis et al., 2020), we estimate individual connectivity loss resulting from white matter lesions by overlapping an automatically generated lesion mask with the tractography atlas and using brain graphs to model an individual structural disconnectome: a brain map representing the affected neuronal connections. In this retrospective multi-centric study, we evaluate the proposed approach, by comparing it as closely as possible with disconnectomes extracted from individual diffusion-based tractography in a subset of patients and we explore its clinical usefulness in reducing the clinico-radiological paradox in multiple sclerosis.

medRxiv preprint doi: https://doi.org/10.1101/2021.05.03.21256161; this version posted May 4, 2021. The copyright holder for this preprint
(which was not certified by peer review) is the author/funder, who has granted medRxiv a license to display the preprint in perpetuity.
It is made available under a CC-BY-NC 4.0 International license .

2. Datasets

Demographics and relevant MR protocol parameters are reported in Table 1 for all cohorts. The number of patients in each dataset corresponds to those fulfilling the applicability criterion defined in Section 3.2.3.

2.1. Diffusion Cohort: controls and patients with diffusion data

Forty-five patients with relapsing-remitting MS (disease duration < 5 years) were scanned on a 3T MRI system (MAGNETOM Trio, Siemens Healthcare, Erlangen, Germany) using a 32-channel head coil at the Lausanne University Hospital (Simioni et al., 2014). The acquisition protocol included: (i) high-resolution magnetization prepared - rapid gradient echo (MPRAGE), (ii) fluid attenuation inversion recovery and (iii) diffusion spectrum imaging (DSI).

T2 hyperintense lesions were manually marked by one radiologist and one neurologist, and a consensus lesion mask was created as described in (Fartaria et al., 2016).

Two patients were discarded due to incomplete imaging data and two other patients did not fulfil the applicability criterion resulting in a subset of forty-one MS patients (13 males, average age 35.1+/-9.86, EDSS ϵ [1,4], median EDSS 1.5 (see Section 3.2.3 for further details). All patients provided written informed consent, and the study was approved by the ethics committee of the State of Vaud, Switzerland.

2.2. 1.5T cohort

An observational Study of Early Interferon beta 1-a Treatment in high risk subjects after clinical isolated syndrome (SET study (Horakova et al., 2013)) recruited 220 patients within four months after their first clinical event suggestive of MS and all eventually converted to clinically definite MS. Patients were scanned at 1.5T (Gyroscan NT 15, Philips Healthcare, Best, The Netherlands) and clinically evaluated every six months during a period of four years. The study involved eight centers and was coordinated by the Charles University Hospital of Prague, where all patients underwent MR examinations. The acquisition protocol included i) fluid attenuation inversion recovery (FLAIR) and ii) T1-weighted spoiled-gradient recalled (SPGR).

An expert neurologist with nine years of experience manually segmented T2 hyperintense lesions in FLAIR. A subset of 208 patients was retained for analysis following our applicability criterion (69 males, average age 28.6+/-7.5, EDSS ϵ [0,3.5], median EDSS 1.5) (see Section 3.2.3).

2.3. 3T cohort

Five hundred eighty-nine patients affected by any form and stage of MS (clinically isolated syndrome, relapsing remitting, secondary progressive and primary progressive) were recruited in a project (the Spinal Cord Grant (SCG)) coordinated by the Charles University Hospital of Prague (Czech Republic). Patients underwent yearly clinical examination and MR imaging at 3T (MAGNETOM Skyra, Siemens Healthcare, Erlangen, Germany). The acquisition protocol included high-resolution magnetization prepared - rapid gradient echo (MPRAGE) and 3D fluid attenuation inversion recovery (FLAIR).

Due to the considerable number of patients, manual segmentations of white matter lesions were not available.

medRxiv preprint doi: https://doi.org/10.1101/2021.05.03.21256161; this version posted May 4, 2021. The copyright holder for this preprint (which was not certified by peer review) is the author/funder, who has granted medRxiv a license to display the preprint in perpetuity. It is made available under a CC-BY-NC 4.0 International license .

Four hundred ninety-six patient datasets fulfilled the applicability criterion (158 males, average age 28 +/- 8.36, EDSS ϵ [0, 7,5], median EDSS 2).

All participants in the 1.5T and the 3T cohorts agreed with collecting and retrospectively analyzing their clinical, immunological and MRI data within an international, online registry and platform for collecting prospective data on patients with MS (MSBase) (Butzkueven et al., 2006), and within the Czech national registry of MS patients (ReMuS). Therefore, neither ethics committee approval nor separate informed consent were obtained for this study. One hundred thirty-two patients were present in both the 1.5T and the 3T cohorts, but were scanned at different time points.

Table 1. Demographics and relevant MR protocols for the three datasets. Lesion volumes are estimated from manual segmentations when available (Diffusion and 1.5T cohorts) and from LeMan-PV otherwise (3T cohort).

		Diffusion cohort	**1.5T cohort**	**3T cohort**
N (Males)		41 (13)	208 (69)	496 (158)
Age [years]		35.1 ± 9.86	28.28 ± 7.31	28.0 ± 8.20
Median EDSS [min,max]		1.5 [1, 4]	1.5 [0, 3.5]	2 [0, 7.5]
Disease Duration [months]		23.78 ± 18	< 3	143 ± 79
Lesion Load [mL]		7.74 ± 9.36	4.19 ± 5.27	13.0 ± 14.6
MR System	Vendor	Siemens	Philips	Siemens
	Scanner	3T Trio	1.5T Gyroscan	3T Skyra
T1w	Voxel size [mm^3]	1x1x1.2	1x1x1	1x1x1
	Acquisition Type	3D	3D	3D
	TR/TE/TI [ms]	2300/2.98/900	25/5/-	2300/2.96/900
	Flip Angle	9°	30°	9°
FLAIR	Voxel size [mm^3]	1x1x1.2	1x1x1.5	1x1x1
	Acquisition Type	3D	2D	3D
	TR/TE/TI [ms]	5000/394/1800	11000/140/2600	5000/397/1800
	Flip Angle	120°	90°	120°
DSI	Voxel size [mm^3]	1x1x3	-	-
	TR/TE [ms]	8600/144	-	-
	b-max [s/mm^2]	8000	-	-

medRxiv preprint doi: https://doi.org/10.1101/2021.05.03.21256161; this version posted May 4, 2021. The copyright holder for this preprint
(which was not certified by peer review) is the author/funder, who has granted medRxiv a license to display the preprint in perpetuity.
It is made available under a CC-BY-NC 4.0 International license .

3. Methods

Due to patient privacy, the clinical data used in this study cannot be made openly available. The Python code used to extract the disconnectome graph and relevant topological metrics from a lesion mask normalized to MNI space is publicly available (https://gitlab.com/acit-lausanne/lesion-disconnectomics), together with pointers to relevant open data as examples. An R based visualisation script is also made available.

3.1. Pre-processing

Lesions were segmented using the LeMan-PV prototype, an automated lesion segmentation technique that performs lesions segmentations on FLAIR and T1-weighted contrasts in two main steps: lesions are first detected using a supervised voxel-wise approach (Fartaria et al., 2016) and then delineated based on partial volume estimation (Fartaria et al., 2017). Lesion concentration maps resulting from LeMan-PV were binarized following the methodology described in (Fartaria et al., 2017), yielding binary lesion masks. LeMan-PV segmentations were computed for the diffusion cohort (in addition to manual segmentation) and the 3T cohort, whereas it was not applied to the 1.5T cohort as the data was not compliant with the minimal requirements defined by LeMan-PV for a good segmentation quality (in particular, data was acquired using a 2D rather than a 3D FLAIR sequence)(Fartaria et al., 2016).

To overlay the lesion mask with the tractography atlas, a non-rigid spatial registration was used to transform the native T1-weighted contrast of each patient to the standard T1-weighted MNI152 (2009a) template space using b-spline trilinear interpolation from the Elastix v.4.800 implementation (Klein et al., 2010) (the parameters file are available in the code repository). The transformation was then applied to the binary lesion mask with nearest neighbour interpolation to ensure binary output mask and preserving lesion topology.

Patients' normalised brains were then segmented in 274 fine-grained subregions using the Brainnetome parcellation atlas (Fan et al., 2016), a connectivity-based atlas extracted with multimodal neuroimaging data from 40 healthy subjects.

3.2. Modelling structural disconnectomes from a tractography atlas

Similarly to the method described in (Griffis et al., 2020), we estimate disconnectomes without diffusion imaging data, using a population-averaged structural tractography atlas, namely the HCP842 tractography atlas (Yeh et al., 2018). The HCP842 atlas was built by averaging the Spin Distribution Function (SDF) in each voxel for 842 healthy subjects from the Human Connectome Project (Van Essen et al., 2012) (372 males, age range between 22 and 36 years old) whose diffusion data was reconstructed in MNI space using a q-space diffeomorphic strategy (Yeh and Tseng, 2011).

3.2.1. Computation of the individual disconnectomes

For each patient, affected connections were extracted by isolating the atlas streamlines passing through the patient's normalised lesion mask using DSI Studio (http://dsi-studio.labsolver.org). Subsequently, the connectivity of affected connections between all possible pairs of brain regions (i, j) extracted from the Brainnetome atlas was modelled as an adjacency matrix of damaged connectivity A_c. Each element of the matrix $A_C(i, j)$ represented the number of damaged streamlines passing through the corresponding pair of regions (i, j).

medRxiv preprint doi: https://doi.org/10.1101/2021.05.03.21256161; this version posted May 4, 2021. The copyright holder for this preprint (which was not certified by peer review) is the author/funder, who has granted medRxiv a license to display the preprint in perpetuity. It is made available under a CC-BY-NC 4.0 International license .

The reference "healthy" brain connectivity was represented as an adjacency matrix A_t where elements $A_t(i,j)$ represented the number of streamlines passing through the corresponding pair of regions (i,j) in the tractography atlas. (see Figure 1A to C and Figure 2A to B). Note that A_t is the same for all patients, while A_c is patient-specific and depends on lesions.

The matrix of affected connectivity A_c was then used to build a brain graph where each parcellation area was represented by one node V_i. Each edge $E(i,j)$ represented the percentage of streamlines affected by lesions connecting areas *i* and *j* with respect to the atlas connectivity $A_t(i,j)$:

$$w_{ij} = \begin{cases} 0, if\ A_t(i,j) = 0 \\ (A_t(i,j) - A_c(i,j))/A_t(i,j), otherwise \end{cases}$$

This weighted graph model ensures the number of nodes is consistent across patients and that the edge weights lie between 0 and 1 (see Figure 1D).

For visualization, a simplified diagram of connection loss was obtained by grouping Brainnetome regions into the main brain lobes and displaying them using Circos (Connors et al., 2009): the line thickness represents the number of affected streamlines whereas the colour codes for the percentage of affected streamlines relative to the healthy atlas (see Figure 2C).

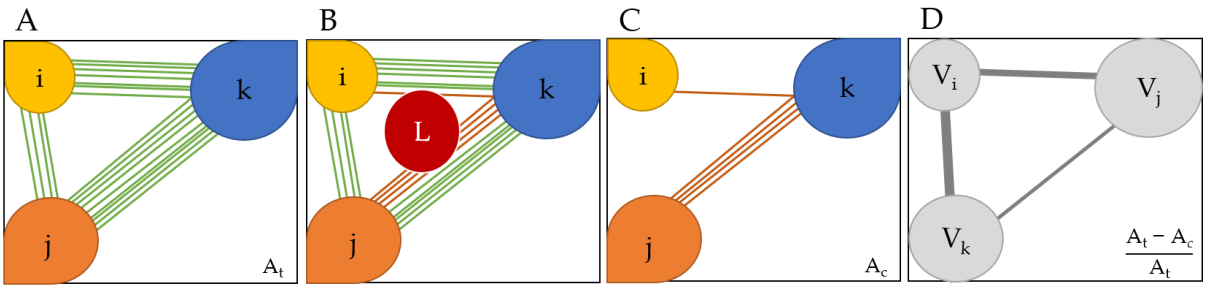

Figure 1. Extraction and modelling of a disconnectome. A. Simplified representation of the atlas-based tractogram connectivity of three brain regions i, j and k and their respective streamlines. B. Overlapping of the atlas tractogram with the lesion mask. Streamlines passing through the lesion L are highlighted in red. C. Affected streamlines are isolated. D. The brain graph representation where brain areas i, j and k are represented respectively by nodes V_i, V_j and V_k and edges are weighted by the relative number of affected streamlines.

3.2.2. Extraction of Graph Features

One way of using graphs for statistical analysis or machine learning is to represent them as vectors, i.e., to use graph embedding. Then, a vast number of algorithms, both classical and deep, can be used without modification for predictive modelling on graphs (Richiardi et al., 2013). Embedding techniques include the extraction of topological features characterizing graph properties, as well as graph representation learning approaches (Hamilton et al., 2017) that optimize the geometric relationships of the embedding in order to reflect graph structure.

medRxiv preprint doi: https://doi.org/10.1101/2021.05.03.21256161; this version posted May 4, 2021. The copyright holder for this preprint
(which was not certified by peer review) is the author/funder, who has granted medRxiv a license to display the preprint in perpetuity.
It is made available under a CC-BY-NC 4.0 International license .

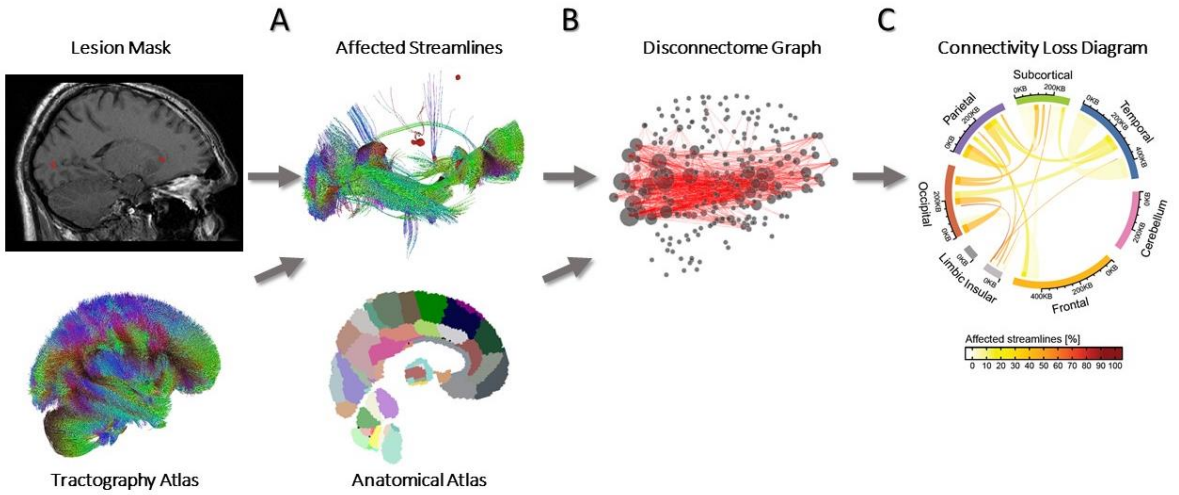

Figure 2 Extraction and representation of a disconnectome. A. The streamlines intersecting the lesion mask are isolated from the healthy tractography atlas. B. Affected streamlines are overlaid with an anatomical atlas to create a brain graph representation of disconnectivity. C. Lobe-wise summary representation of disconnectivity, visualized using Circos (Connors et al., 2009).

Topological graph features can be defined at different scales: at large-scale, they reflect properties on the entire graph (e.g. small-worldness), at intermediate scale, the metrics are computed on subgraphs (e.g. edge betweenness) and at small scale they reflect node features (e.g. node strength) (De Vico Fallani et al., 2014). Here, we extracted different small- and large-scale features computed with the NetworkX Python library (Hagberg et al., 2008) to study both the performance of our atlas-based method compared to individual disconnectomes, and the usefulness of these metrics for clinical applications. The topological features used are described in

Further, the averages of strength, neighbour degree, clustering coefficient and betweenness centrality were also computed across all nodes.

We use transitivity (T), global efficiency (GE), and path length (PL) as defined for binary graphs, and the disconnectome graphs were binarized using a threshold τ on edge weights so that the most severely affected connections were modelled as totally disrupted, and the mildly affected ones were modelled as intact. Binary edges were therefore defined such as:

$$w_{ij}^{bin} = \begin{cases} 1, if\ w_{ij} \geq \tau \\ 0, otherwise \end{cases}$$

We checked that graphs remained connected after thresholding and artificially added one edge to reconnect eventual disconnected components. A detailed analysis aiming at defining the optimal binarization threshold for disconnectome graphs is described in Supplementary Materials Appendix C and resulted in a threshold of 0.7.

Node embeddings were also extracted from the disconnectome graph using node2vec, a graph learning representation technique. Node2vec (Grover and Leskovec, 2016) leverages a random walk sampling strategy to optimize an embedding that is similar for nodes that tend to co-occur in short random walks. The parameters used for node2vec embeddings are reported in Supplementary Materials Appendix A.

medRxiv preprint doi: https://doi.org/10.1101/2021.05.03.21256161; this version posted May 4, 2021. The copyright holder for this preprint (which was not certified by peer review) is the author/funder, who has granted medRxiv a license to display the preprint in perpetuity. It is made available under a CC-BY-NC 4.0 International license .

Table 2 Description of topological metrics extracted from the disconnectome graph. In the following equations V is the set of nodes, $\sigma(j,k)$ is the number of shortest paths between nodes j and k, $\sigma(j,k|i)$ is the number of those paths passing through node i, $\mathcal{N}_i$ is the set of nodes in the neighbourhood of node i, $\hat{w}_{ij}$=$\frac{w_{ij}}{max\,(w)}$ and k_i the node degree defined as the number of edges connecting to node i. $p(i,j)$ the shortest path length between nodes i and j and with n=274 the number of nodes in the graph.

Group	Features	Source	Equation	Binary
Small-scale	Betweenness Centrality	(Brandes, 2001)	$bc_i = \sum_{j,k \in V} \frac{\sigma(j,k\|i)}{\sigma(j,k)}$	NO
	Node Strength	(Vespignani et al., 2004)	$s_i = \sum_{j \in \mathcal{N}_i} w_{ij}$	NO
	Clustering Coefficient	(Saramäki et al., 2007)	$c_i = \begin{cases} 0, \; if \; k_i < 2 \\ \frac{1}{k_i(k_i-1)} \sum_{i,j} \left(\hat{w}_{ij}\hat{w}_{ik}\hat{w}_{jk}\right)^{1/3}, \; otherwise \end{cases}$	NO
	Average Neighbour Degree	(Vespignani et al., 2004)	$k_{nn,i} = \frac{1}{s_i} \sum_{j \in \mathcal{N}_i} w_{ij} k_j$	NO
	Transitivity	(Faust, 1994)	$T = \frac{3 \times \text{number of triangles in G}}{\text{number of connected triplets of nodes in } G}$	YES
Large-Scale	Average Global Efficiency	(Latora and Marchiori, 2001)	$GE = \frac{1}{n(n-1)} \sum_{i,j \in V} \frac{1}{p(i,j)}$	YES
	Average Shortest Path Length	(Dijkstra, 1959)	$PL = \sum_{i,j \in V} \frac{p(i,j)}{n(n-1)}$	YES

3.2.3. Model Assumptions and Applicability Conditions

Our proposed model relies on the assumption that a patient's brain connectivity can be estimated from the HCP842 atlas. However, the effects of brain atrophy on axonal projections are unclear and might lead to interpretation issues when approximating atrophic brains with the HCP842 atlas. In fact, brain atrophy, resulting from the loss of neurons or neuronal connections, potentially leads to substantial quantitative changes in structural connectivity (Kuceyeski et al., 2015).

To be coherent with our initial assumption and avoid possible misinterpretation resulting from the presence of atrophy, we used an applicability criterion to discard unsuitable patients. As brain atrophy can be caused either by normal aging or pathology, we implemented a criterion based on both age and brain volume relative to total intracranial volume (TIV) estimated with the MorphoBox prototype brain morphometry software (Schmitter et al., 2015).

First, the quality of the MorphoBox segmentation was assessed to discard patients with unreliable brain volume estimates. The segmentation quality was computed as the correlation between the grey matter a posteriori (GM) probability map generated by MorphoBox and a

medRxiv preprint doi: https://doi.org/10.1101/2021.05.03.21256161; this version posted May 4, 2021. The copyright holder for this preprint
(which was not certified by peer review) is the author/funder, who has granted medRxiv a license to display the preprint in perpetuity.
It is made available under a CC-BY-NC 4.0 International license .

priori GM probability map. Correlations higher than 0.68 were thought to reflect high segmentation quality according to (Chow and Paramesran, 2016). In case of low segmentation quality, brain volume and segmentation quality were assessed for scans in subsequent timepoints and the first scan with sufficiently high segmentation quality was retained as reference. Then, age- and gender-matched MorphoBox reference ranges were used to detect abnormal brain volume in patients belonging to the tractography atlas age range (22 to 36 years old). The 3% and 97% percentiles of normative ranges were chosen not to be too conservative as the sharp boundaries of the atlas age range were already considered. For patients outside this age range, an upper and a lower bound were defined for patients below twenty-two and above thirty-six years old, respectively. The upper and lower bounds were defined as the normative value of the 3% at age twenty-two and thirty-six, respectively.

A flow diagram showing the applicability criterion of our proposed method is represented in Figure 3. The precise breakdown of datasets after applying our applicability conditions is reported in Supplementary Table 1.

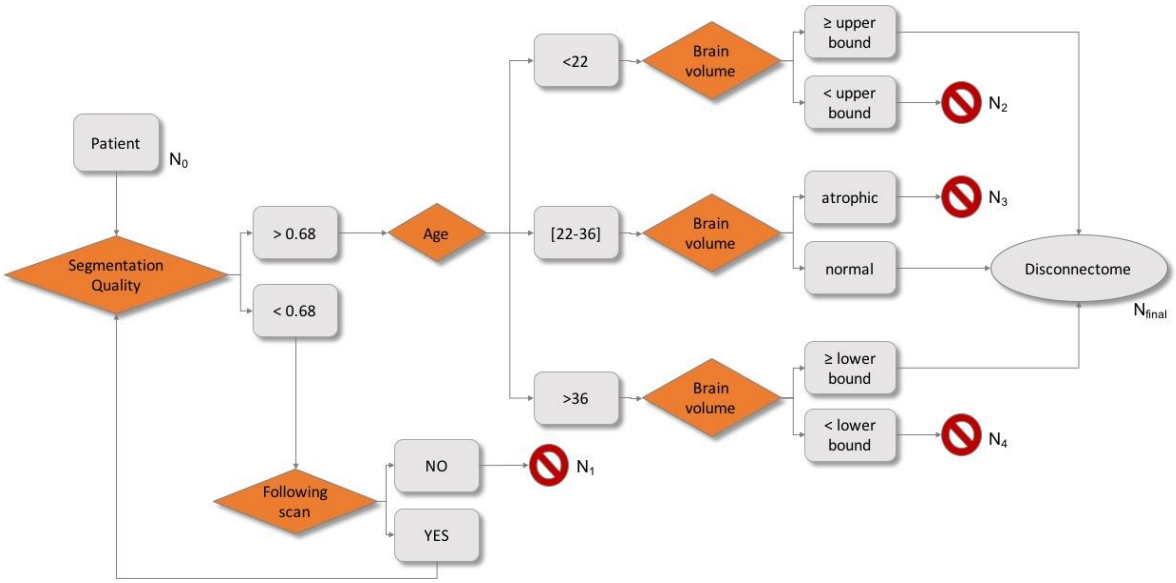

Figure 3. Flow diagram showing the applicability conditions of the atlas-based disconnectome model, based on age, brain atrophy and brain segmentation quality estimated from MorphoBox (Schmitter et al., 2015). N_0: initial number of patients. N_1: number of patients discarded due to bad segmentation quality. N_2: number of patients younger than the age range covered by the tractography atlas, who are discarded due to severe atrophy. N_3: number of patients inside the atlas age range discarded due to atrophy. N_4: number of patients older than the age range covered by the tractography atlas, who are discarded due to mild to severe atrophy.

3.3. Comparison with disconnectomes based on individual tractography

Individual variability in brain connectivity in patients can be either caused by individual anatomical factors or by pathological phenomena such as brain atrophy, oedema, or white and gray matter lesions, degree of de- and remyelination. To estimate the error made under the assumption that patients´ brain connectivity could be approximated with the population-averaged HCP842 tractography atlas, we compared atlas-based disconnectome graphs to the equivalent graphs derived from individual tractography in our diffusion cohort.

medRxiv preprint doi: https://doi.org/10.1101/2021.05.03.21256161; this version posted May 4, 2021. The copyright holder for this preprint
(which was not certified by peer review) is the author/funder, who has granted medRxiv a license to display the preprint in perpetuity.
It is made available under a CC-BY-NC 4.0 International license .

3.3.1. Modelling Disconnectomes from Individual Tractography

To ensure consistency with the HCP842 tractography atlas, the same reconstruction strategy and tracking algorithm were used to build individual whole-brain tractograms as described in (Yeh et al., 2018). All reconstruction and tracking parameters were chosen following (Yeh et al., 2018) and are described in Supplementary Materials Appendix B.

The disconnectome was then extracted and modelled following the same procedure as shown in Section 3.2.1 and will be hereafter referred to as individual tractography-based disconnectome, as opposed to the atlas-based disconnectome.

3.3.2. Comparing Individual Tractography based and Atlas based disconnectomes

To study the impact of using a tractography atlas rather than individual tractography on graph features, a connection-level comparison of disconnectomes was first performed. To this end, lobe-wise connections in the atlas-based and individual tractography-based disconnectome matrices were ranked according to their connectivity strength and rank-rank Spearman correlation was computed for both lesion segmentation techniques in the diffusion cohort.

Correlations between large-scale topological metrics extracted from both disconnectome models were investigated on the population level in the diffusion cohort by computing the intraclass correlation coefficient (ICC(3,1)) and Spearman's correlation. Then, the ICC and Spearman's correlation between small-scale topological features derived from the two approaches were calculated for each patient independently. The impact of total lesion volume on patient-level correlations was also studied.

Small-scale topological features were extracted for all 274 nodes from atlas-based and individual tractography-based disconnectomes and the intraclass correlation ICC(3,1) and Spearman correlation were computed for each patient in the diffusion cohort and each lesion segmentation strategy.

3.4. Clinical Applications in Multiple Sclerosis

To test the clinical relevance of our technique, we investigated the potential of atlas-based disconnectome features to reduce the gap between radiological findings and physical disability in Multiple Sclerosis. To this end, the usefulness of our features in disease characterization was evaluated and compared to conventional MRI variables reflecting lesion load (i.e., lesion count and lesion volume).

To verify that the extracted topological features were related to actual physiological phenomena instead of measurement noise, the variation of large-scale topological features with total lesion volume was analysed in all cohorts. The analysis was restricted to patients with a TLV smaller than 50 mL to provide a comparable range of TLV between datasets and therefore discarding 15 patients from the 3T cohort. Then, the univariate Spearman's correlation between these features and EDSS was investigated cross-sectionally.

The clinical usefulness of node2vec embeddings in estimating association with cross-sectional EDSS was also studied and contrasted to using standard lesion load measurements in all cohorts. To this end, a supervised dimensionality reduction embedding technique called Uniform Manifold Approximation and Projection (UMAP) was used (McInnes et al., 2018) on node2vec embeddings, to test relation with EDSS. The three main parameters, namely the

medRxiv preprint doi: https://doi.org/10.1101/2021.05.03.21256161; this version posted May 4, 2021. The copyright holder for this preprint
(which was not certified by peer review) is the author/funder, who has granted medRxiv a license to display the preprint in perpetuity.
It is made available under a CC-BY-NC 4.0 International license .

distance metric, the minimal distance, and the number of neighbours, were varied in a grid search approach and the best combination was chosen qualitatively. The minimal distance and the number of neighbours were varied in a range between 0.5 and 1, and between 32 and max(n,256) respectively, with n the number of patients in the dataset. Euclidean, Dice and Hamming distances were explored. Patient data was then plotted onto the two UMAP dimensions and color-coded according to EDSS for all cohorts.

Finally, to further study the clinical usefulness of our approach, patients were stratified according to global efficiency of their remaining connectivity and their lesion load. In particular, for every cohort, patients had low lesion load when their total lesion volume (TLV) was below the average TLV within their cohort. Similarly, patients had low, or high global efficiency with respect to the average value within each cohort. The EDSS distribution was then compared between the four groups for each cohort and tested for significance using non-parametric Wilcoxon test. The so-obtained p-values were further combined in a metanalysis using sum of z method.

4. Results

4.1. Comparing Disconnectome Models

The connection-level rank-rank Spearman correlation between atlas-based and individual tractography disconnectomes computed in patients from the diffusion cohort was 0.76±0.07 and 0.75±0.07 for automated and manual lesion segmentation respectively and is shown in Supplementary Figure 2.

4.1.1. Large-scale Topological Features

Large-scale topological features extracted from atlas-based disconnectome graphs were plotted against equivalent features derived from individual tractography-based disconnectomes in Figure 4 for both manual segmentation (in yellow) and automated LeMan-PV segmentation (in blue) for the diffusion cohort. Intraclass correlation ICC(3,1) and Spearman correlation between large-scale atlas-based and individual tractography-based features in the diffusion cohort, extracted with both manual and automated LeMan-PV segmentations are reported together with significance level after Benjamini-Hochberg false discovery rate (FDR) correction. Overall, manual segmentation allowed a slightly stronger although similar correlation between atlas-based and individual tractography-based features.

Spearman's correlation was above 0.8 for all features but average neighbour degree and average betweenness centrality with both lesion segmentation strategies. ICC was higher for transitivity, average clustering, and average strength (>0.6). Comparatively small ICC (<0.4) were observed not only for average betweenness centrality and average neighbour degree, but also for global efficiency and average shortest path length.

medRxiv preprint doi: https://doi.org/10.1101/2021.05.03.21256161; this version posted May 4, 2021. The copyright holder for this preprint
(which was not certified by peer review) is the author/funder, who has granted medRxiv a license to display the preprint in perpetuity.
It is made available under a CC-BY-NC 4.0 International license .

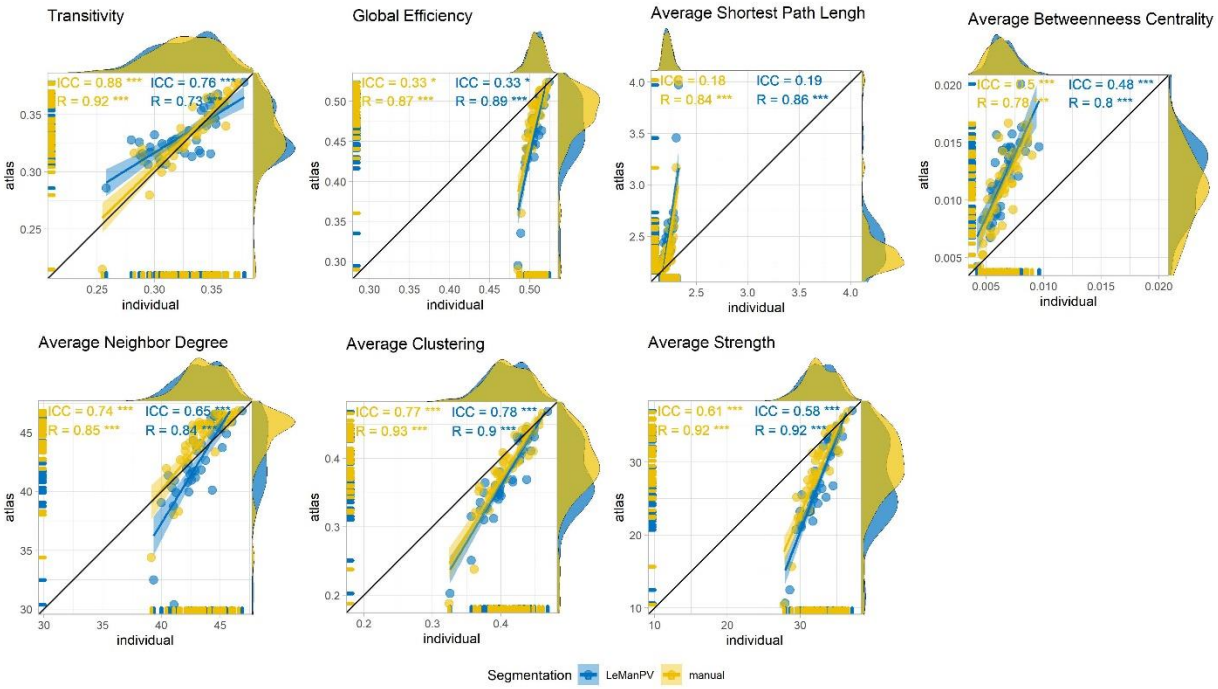

Figure 4. Large scale topological features extracted from atlas-based disconnectome graph (y-axis) plotted against equivalent metrics extracted from individual tractography-based disconnectome (x-axis) for patients of the diffusion cohort. Each point is a patient. Disconnectome features derived from manual lesion segmentation are shown in yellow, and automated lesion segmentation with LeManPV in blue. ICC(3,1) and Spearman's correlation are reported with their respective significance level after correction for multiple comparison. * p<0.05, ** p<0.01, *** p<0.001

4.1.2. Small-scale Topological Features

Average correlations and standard deviation computed across all patients are reported in Table 3, together with combined p-values using Fisher's method and respective χ^2 statistics. Overall, the results show that atlas-based features are highly correlated with individual tractography-based features (ICC>0.75, ρ>0.75), except for the betweenness centrality (ICC<0.25, ρ<0.6), in good accordance with previous observations in Section 4.1.1. Further, automated lesion segmentation did not substantially impact the correlation between atlas-based and individual tractography-based features.

medRxiv preprint doi: https://doi.org/10.1101/2021.05.03.21256161; this version posted May 4, 2021. The copyright holder for this preprint (which was not certified by peer review) is the author/funder, who has granted medRxiv a license to display the preprint in perpetuity. It is made available under a CC-BY-NC 4.0 International license .

Table 3 Intraclass correlation and Spearman ρ between small-scale atlas-based and Individual tractography-based small-scale features and the associated p-value adjusted for FDR, for both manual and automated LeMan-PV lesion segmentation. The ICC is expressed as the mean over the population ± standard deviation. P-values were combined using Fisher's method across the population. The combined p-value is reported together with the respective χ^2 statistics

	Node strength		**Neighbour degree**		**Node Clustering**		**Betweenness Centrality**	
Segmentation	Manual	LeMan-PV	Manual	LeMan-PV	Manual	LeMan-PV	Manual	LeMan-PV
ICC	0.85±0.16	0.76±0.2	0.90±0.08	0.86±0.12	0.87 ± 0.8	0.84 ± 0.08	0.20±0.1	0.19±0.08
P (χ^2_{ICC})	$<10^{-16}$ (19550)	$<10^{-16}$ (14898)	$<10^{-16}$ (19905)	$<10^{-16}$ (17875)	$<10^{-16}$ (17905)	$<10^{-16}$ (15698)	$<10^{-16}$ (724)	$<10^{-16}$ (647)
ρ	0.86±0.14	0.78±0.18	0.90±0.09	0.85±0.15	0.76±0.14	0.70±0.16	0.54±0.12	0.52±0.10
p (χ^2_{ρ})	$<10^{-16}$ (19136)	$<10^{-16}$ (15024)	$<10^{-16}$ (20691)	$<10^{-16}$ (17192)	$<10^{-16}$ (11442)	$<10^{-16}$ (9350)	$<10^{-16}$ (4376)	$<10^{-16}$ (3973)

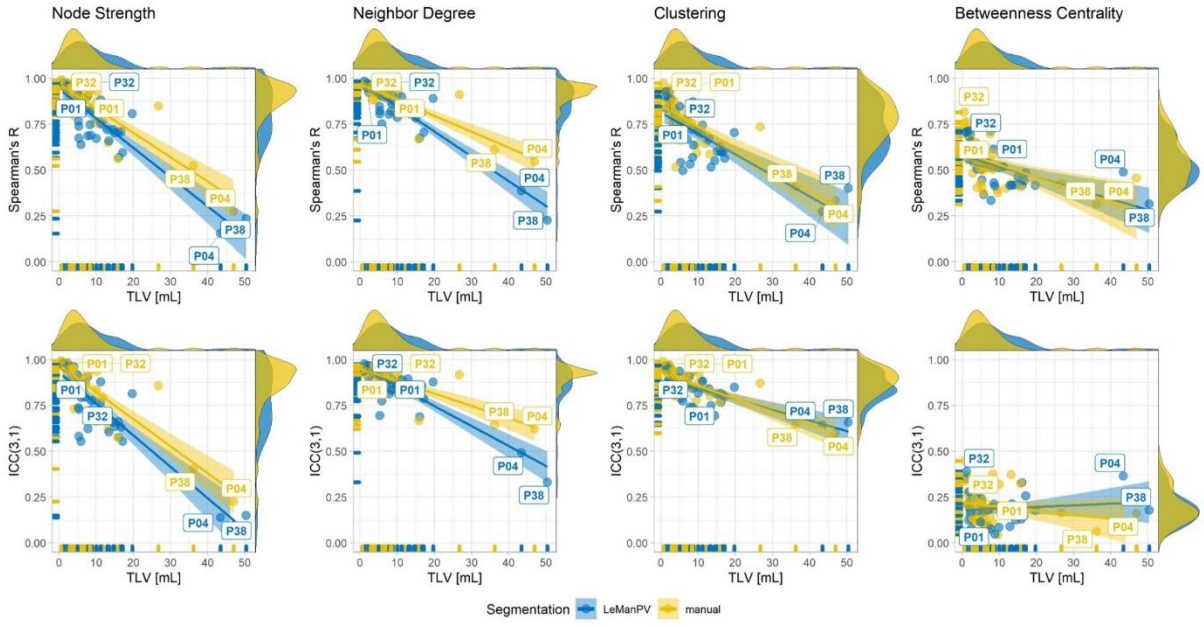

Figure 5. Variation of correlation of small-scale features extracted from individual versus atlas-based tractography with lesion load for the diffusion dataset. Each point is a patient. Spearman correlation and ICC(3,1) agreement between the two methods are computed across nodes for all patients and are shown on the y-axis. The total lesion volume (TLV) estimated from either manual (in yellow) or LeMan-PV lesion segmentations (in blue) on the x-axis. Labels in the graph indicate patient with generally high or low agreement, for which details are provided in supplementary materials.

medRxiv preprint doi: https://doi.org/10.1101/2021.05.03.21256161; this version posted May 4, 2021. The copyright holder for this preprint
(which was not certified by peer review) is the author/funder, who has granted medRxiv a license to display the preprint in perpetuity.
It is made available under a CC-BY-NC 4.0 International license .

Figure 5. Figure 5 shows how intraclass correlation and Spearman correlation vary with TLV estimated from either manual segmentation (in yellow) or LeMan-PV (in blue). Overall, the weakest correlations were observed for larger lesion loads and segmentation techniques did not substantially impact the correlation distributions.

In Supplementary Figure 3 two patients with overall high correlations (P01 and P32) and low lesion load are shown together with two patients with overall lower correlations (P04 and P38) and higher lesion load.

4.2. Clinical Applications

4.2.1. Disease Characterization

The variation of large-scale topological features with the TLV (estimated from manual segmentation for the diffusion and the 1.5T datasets and from LeMan-PV for the 3T dataset) is represented in Figure 6 for patients in the three datasets. As betweenness centrality and neighbour degree were shown to be poorly estimated with our atlas-based approach, these metrics were discarded from further analysis. Overall, patients in the 1.5T cohort had lower lesion load than other patients. All features showed strong and significant Spearman correlations with TLV in all datasets. The weakest correlations were observed for the transitivity, especially when computed for the 3T cohort (R=-0.42), and average neighbour degree in all cohorts (R<0.62). Transitivity, global efficiency, average clustering, average strength, and average neighbour degree were found to decrease with increasing lesion load, whereas the average shortest path length increased.

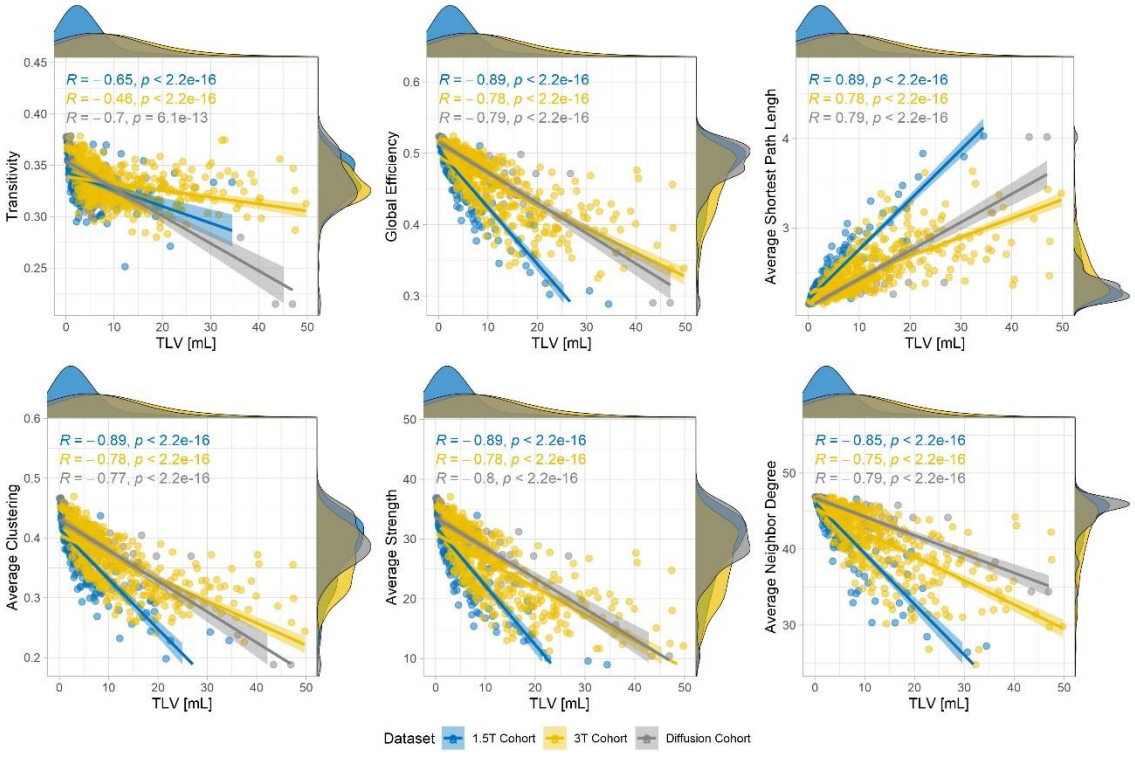

Figure 6 Variation of large scale topological features (y-axis) with total lesion volume (TLV, x-axis) for patients in all datasets (diffusion cohort in grey, 1.5T cohort in blue and 3T cohort in yellow). Spearman's R and p-value are reported for all datasets.

medRxiv preprint doi: https://doi.org/10.1101/2021.05.03.21256161; this version posted May 4, 2021. The copyright holder for this preprint
(which was not certified by peer review) is the author/funder, who has granted medRxiv a license to display the preprint in perpetuity.
It is made available under a CC-BY-NC 4.0 International license .

The variation of large-scale features is also plotted against EDSS in Figure 7 for the three datasets. For comparison, the correlation between variables reflecting the lesion load (lesion count and TLV) and the EDSS are also reported. Patients in the 3T dataset had overall more severe and more heterogeneous EDSS than patients in the 1.5T and diffusion datasets. Lesion count and TLV were comparably correlated with EDSS for all datasets. The weakest correlations were consistently observed for the 1.5T dataset, whereas the findings were generally in good accordance between the 3T and the diffusion datasets. Overall, the correlation between our topological variables and EDSS was comparable but not substantially stronger than the correlations with TLV and lesion count.

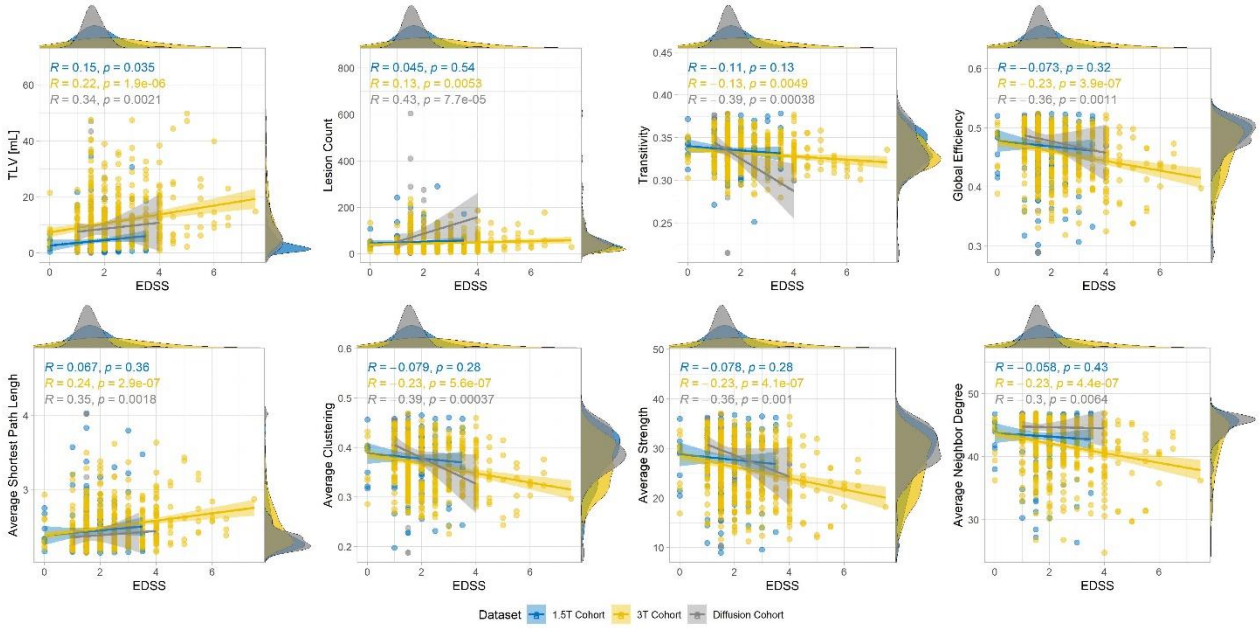

Figure 7 Variation of large scale topological features (y-axis) with Expanded Disability Status Scale (EDSS, x-axis) for patients in all datasets (diffusion cohort in grey, 1.5T cohort in blue and 3T cohort in yellow). Spearman's R and p-value are reported for all datasets.

The results of UMAP embedding of node2vec features are shown in Figure 8, where patients' data is displayed in the two UMAP dimensions and color-coded by EDSS value. Patients from the 1.5T and 3T cohort were found to follow an EDSS gradient in the latent space, and patients with higher EDSS were formed a separate cluster in the 3T cohort. We did not observe this in the diffusion cohort patients, probably due to the insufficient number of patients to train the embedding. The best results were obtained for Euclidean distance, with a minimal distance of 0.7 and respectively 256, 128 and 32 nearest neighbours for the 3T, the 1.5T and diffusion datasets.

For comparison, when performing the embedding from lesion load variables and attempting to obtain the best tuning, neither a gradient nor a clustering of EDSS values could be observed in any dataset.

medRxiv preprint doi: https://doi.org/10.1101/2021.05.03.21256161; this version posted May 4, 2021. The copyright holder for this preprint
(which was not certified by peer review) is the author/funder, who has granted medRxiv a license to display the preprint in perpetuity.
It is made available under a CC-BY-NC 4.0 International license .

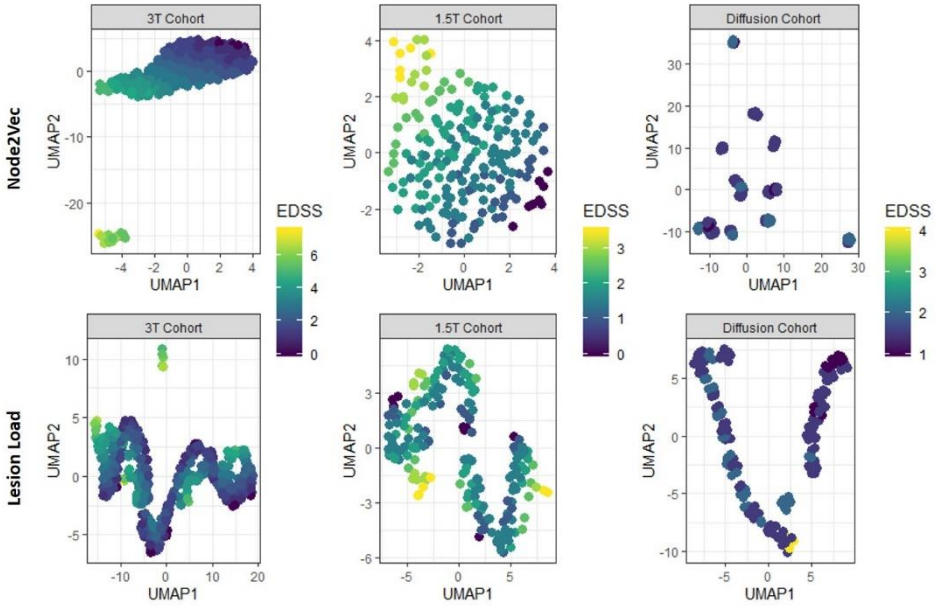

Figure 8. Results of supervised Uniform Manifold Approximation and Projection (UMAP) using EDSS as labels for: (left) the 3T, (middle) 1.5T and (right) Diffusion datasets based on (top) node2vec embeddings and (bottom) lesion load and lesion count features. Datapoints are color-coded by EDSS value.

When stratified according to TLV and global efficiency, patients consistently showed significantly different EDSS across datasets (see Figure 9). In particular, among patients with low TLV, those who were also characterized by a low global efficiency had more severe EDSS than those with higher global efficiency (3T cohort p=0.0088, diffusion cohort p=0.036 and for 1.5T cohort p=0.018). These findings were also significant when combined in a meta-analysis (sumz=3.93, $p=10^{-5}$). The cut-off used to stratify patients according to their TLV and global efficiency (GE) are reported in Supplementary Table 2 for each cohort.

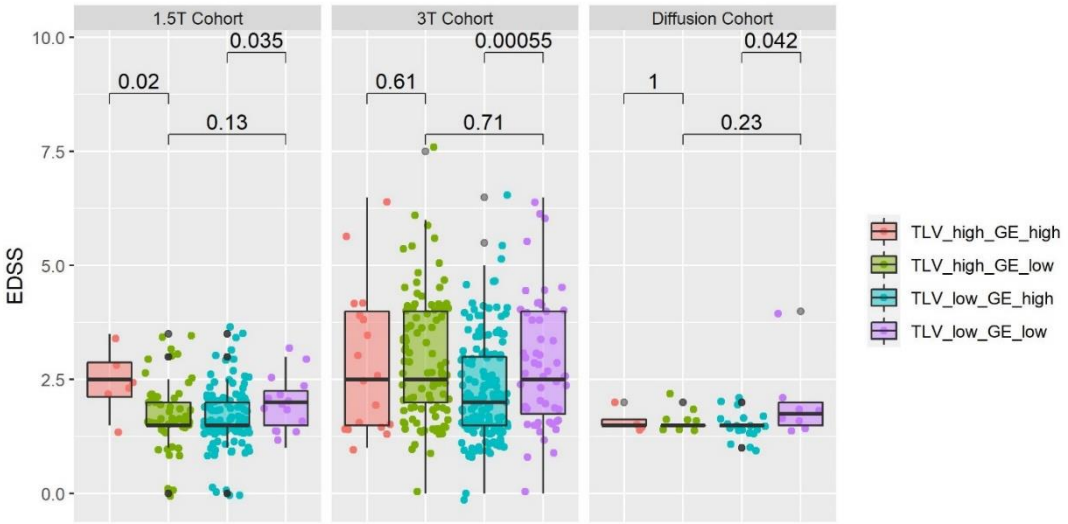

Figure 9. EDSS distribution in all cohorts when stratified according to total lesion volume (TLV) and the global efficiency (GE) of their remaining connectivity. The cut-offs used to classify patients were the average TLV and GE within each cohort. These cut-offs are reported in Supplementary Table 2.

medRxiv preprint doi: https://doi.org/10.1101/2021.05.03.21256161; this version posted May 4, 2021. The copyright holder for this preprint
(which was not certified by peer review) is the author/funder, who has granted medRxiv a license to display the preprint in perpetuity.
It is made available under a CC-BY-NC 4.0 International license .

5. Discussion

In this work, we validated a novel approach to model structural disconnectomes without diffusion imaging in a large retrospective multi-centric study of multiple sclerosis. Similarly to what has been described in (Griffis et al., 2020), the HCP842 tractography atlas (Yeh et al., 2018) was used to extract brain connections transected by lesions, and the remaining connectivity was modelled as a brain graph. Contrary to “lesion network mapping”, our method allows to quantify the impact of lesions on the whole structural connectome instead of focusing on specific sub-networks. Disconnectome topological features and node embeddings were proposed as possible new imaging biomarkers.

The connection-level rank correlation between atlas-based and individual tractography-based models suggests that the strength of connections is overall consistently reflecting a substantial similarity between disconnectome graphs.

Topological features extracted from atlas-based disconnectomes and classical individual models were strongly correlated and suggest that our atlas-based model is a well-suited approximation of individual connectivity loss. Overall, atlas-based features were strongly correlated to individual tractography-based features, even though an offset was often observed, showing consistency if not absolute agreement. In terms of comparability between atlas-based and individual tractography-based methods, betweenness centrality and neighbour degree were the worst performing features on both small- and large-scale levels. This observation suggests that our atlas-based method is reflects well global or node properties that are independent from specific paths, whereas it does not allow a precise approximation of node neighbourhood. This could be explained by normal individual variability in axonal connections and by the erroneous or biased estimation of disconnectomes from individual tractography (e.g., presence of false positive streamlines). Using an automated lesion segmentation did not negatively impact the results, suggesting that a fully automated approach could be used to estimate disconnectome graphs using LeMan-PV segmentation estimated solely from T1-weighted and FLAIR contrasts.

When comparing atlas-based to individual tractography-based disconnectomes in MS patients, one should take into consideration that although the same reconstruction and tracking algorithms were used as for the tractography atlas, individual tractograms lacked the filtering of false positives which was performed manually during the construction of the atlas. Furthermore, our disconnectome method assumes that streamlines affected by lesions can be isolated from the structural connectome. However, individual tractography can already be influenced by the presence of lesions itself (Lin et al., 2005; Reich et al., 2007; Tievsky et al., 1999) and might not therefore reflect the actual structural connectivity of these patients.

Large-scale atlas-based topological features were shown to be significantly correlated with total lesion volume in all datasets. Importantly, the association between TLV and topological features was assumed to be linear, but other distributions could be better suited to reflect this correlation, especially for transitivity and average clustering which seem to follow a logarithmic function. These observations were coherent for all datasets despite substantial differences in terms of demographics, lesion load and clinical scores. However, different brain parcellation techniques might influence the graph properties due to different definitions of a “node” and should be explored in future work. In general, a greater variability is expected to be induced by smaller brain regions, leading to a bias-variance trade-off.

medRxiv preprint doi: https://doi.org/10.1101/2021.05.03.21256161; this version posted May 4, 2021. The copyright holder for this preprint
(which was not certified by peer review) is the author/funder, who has granted medRxiv a license to display the preprint in perpetuity.
It is made available under a CC-BY-NC 4.0 International license .

In multiple sclerosis patients, values decreased for increasing lesion load for transitivity, average clustering, average strength, and global efficiency, whereas the average shortest path length increased, resulting in decreased small-worldness. This is consistent with previous studies (Aerts et al., 2016; Faivre et al., 2016; Rocca et al., 2016, 2015) that showed significantly lower node strength, efficiency, clustering and increased shortest path length in MS patients when compared to controls (Shu et al., 2016), and impaired small-world efficiency associated to white matter lesion load. Interestingly, the distribution of topological measures were closer between the 3T and diffusion cohorts despite different lesion segmentation strategies. Such observation could be explained by the different lesion load distribution of the 1.5T cohort and the substantially different acquisition protocols.

Univariate correlations between large-scale topological features and EDSS were generally poor but close to lesion load variables. Previous studies showed a significant decrease in global efficiency although weakly correlated with EDSS (Muthuraman et al., 2016; Shu et al., 2011). Weaker correlations were observed for the 1.5T dataset, probably due to the narrower distribution of EDSS values. When fed to a supervised UMAP algorithm, node2vec embeddings allowed to define a two-dimensional space where patients followed an EDSS gradient for the 1.5T and 3T cohorts. A cluster of more severely disabled patients was also found in the 3T cohort based on the UMAP dimensions. The smaller number of patients in the diffusion cohort did not allow to observe such gradient clearly. When performed on lesion load variables, the UMAP algorithm did not allow to organize patients according to an EDSS gradient. The larger number of variates in node2vec embeddings compared to lesion load should be taken into consideration and might partially explain these results.

When stratified according to their TLV and global efficiency, patients with low lesion load showed significantly different EDSS depending on their global efficiency value: the lower the global efficiency, the worst the clinical outcome. These findings were validated across all cohorts and suggest that disconnectome topological features could be used in addition to TLV to stratify patients into subgroups reflecting different clinical states. In patients with high TLV, significantly higher EDSS values were observed for higher global efficiency in the 1.5T cohort. A high remyelination capacity might explain these results since the 1.5T cohort was composed by patients at very early stages of the disease. Another hypothesis to explain these findings is the interplay of other pathophysiological effects we are not considering, such as the influence of spinal cord and optic nerve lesions on EDSS.

Due to the limited age range covered by the tractography atlas, we implemented an applicability criterion that restricts the target clinical population to patients without profound atrophy. Therefore, the findings of this work must be interpreted accordingly and cannot be extrapolated to all multiple sclerosis patients. In addition to global brain atrophy, regional atrophy levels might also impact the anatomy of neuronal connections and should be deeper investigated in future work. Also, the contribution of brain plasticity which might yield to a partial or complete recovery of neuronal connections (Aerts et al., 2016; Fleischer et al., 2019; Rocca et al., 2015) is not considered in our atlas-based approach, and could impact the correlation with clinical scores.

Different types of lesions might differently impact the connectivity loss based on their active or inactive state, as well as ongoing remyelination and demyelination processes. Future work should aim at investigating this relation using contrast enhanced scans to identify active lesions, whilst T1 hypointensities could be used to find “black holes”.

medRxiv preprint doi: https://doi.org/10.1101/2021.05.03.21256161; this version posted May 4, 2021. The copyright holder for this preprint
(which was not certified by peer review) is the author/funder, who has granted medRxiv a license to display the preprint in perpetuity.
It is made available under a CC-BY-NC 4.0 International license .

Another limitation of our approach is that it only considers connectivity changes in response to focal WM lesions. However, WM lesions are only a part of the complex pathophysiology of MS, and other mechanisms might also influence connectivity impairments, such as microstructural damage in normal appearing white matter (Solana et al., 2018). Further, lesions located in the spine, cortex and optical nerve were not considered in this study but might play a role in explaining the clinico-radiological paradox in multiple sclerosis.

Previous studies have shown how brain connectivity and network efficiency in particular can be affected by the sex and brain size of the subject (Yan et al., 2011). Such effects are not considered in our approach as the tractography atlas is independent form the sex and brain size, which might therefore result into interpretation pitfalls.

6. Conclusion

In conclusion, our atlas-based graph model of disconnectivity allows to extract topological features shown to reflect actual physiological properties and in good accordance with individual tractography disconnectome models in multiple sclerosis. Such metrics were shown to contribute to narrowing the clinico-radiological gap in multiple sclerosis by providing a new quantitative characterization of brain disconnectivity, in a large retrospective multi-centric study involving substantially different clinical cohorts and MR images in terms of hardware and acquisition sequences.

This method could be applied to any other neurological diseases characterized by the appearance of white matter lesions to study their impact on structural connectivity without requiring diffusion imaging. This is especially interesting for clinical research, as our method enables the retrospective analysis of structural disconnectivity in pre-existing datasets with routine MR contrasts that does not contain high quality diffusion imaging.

Funding

1.5T cohort: SET study; Contract grant sponsor: the Ministries of Health and Education, Czech Republic; EudraCT number: 2005-001281-13; NCT number: NCT01592474; Contract grant numbers: RVO 64165/2012, MSM0021620849; PRVOUK-P26/LF1/4; 3T cohort: Spinal Cord Grant (SCG); Contract grant sponsor: the Ministry of Health, Czech Republic; Contract grant numbers: NV18-04-00168, RVO 64165; Diffusion cohort: Swiss National Science Foundation; Contract grant number: PZ00P3_131914/11; Contract grant sponsor: Centre d'Imagerie Bio-Medicale (CIBM) of the University of Lausanne (UNIL); Contract grant sponsor: Centre Hospitalier Universitaire Vaudois (CHUV).

The funding sources had no role in study design; in the collection, analysis, and interpretation of data; in the writing of the report or in the decision to submit the paper for publication.

Acknowledgments

We thank Frank Yeh, author of the tractography atlas and developer of DSI Studio, for the fruitful discussion and his advice on the reconstruction and tracking algorithms used. We also thank Dimitri Van De Ville for gracefully hosting this project and providing useful feedback and discussion.

medRxiv preprint doi: https://doi.org/10.1101/2021.05.03.21256161; this version posted May 4, 2021. The copyright holder for this preprint (which was not certified by peer review) is the author/funder, who has granted medRxiv a license to display the preprint in perpetuity. It is made available under a CC-BY-NC 4.0 International license .

Disclosure

Veronica Ravano: Pending Patent Application; **Michaela Andelova:** received financial support for conference travel from Novartis, Genzyme, Merck Serono, Biogen Idec and Roche; **Mário João Fartaria**: Employee of Siemens Healthcare AG; **Bénédicte Maréchal:** Employee of Siemens Healthcare AG; **Tomas Uher**: received financial support for conference travel and honoraria from Biogen Idec, Novartis, Roche, Genzyme and Merck Serono, as well as support for research activities from Biogen Idec and Sanofi (GZ-2017-11718); **Jan Krasensky:** received financial support for research activities from Biogen Idec; **Manuela Vaneckova:** was supported by Czech Ministry of Health, grant RVO-VFN 64165, NV18-04-00168. She received compensation for speaker honoraria, travel and consultant fees from Biogen, Sanofi Genzyme, Novartis, Roche and Teva, as well as support for research activities from Biogen. **Dana Horakova**: received compensation for travel, speaker honoraria and consultant fees from Biogen, Novartis, Merck, Bayer, Sanofi, Roche, and Teva, as well as support for research activities from Biogen. She was also supported by the Czech Ministry of Education project Progress Q27/LF1. **Jonas Richiardi:** Employee of Siemens Healthcare AG and Pending Patent Application; **Tobias Kober:** Employee of Siemens Healthcare AG and Pending Patent Application. The other authors have nothing to disclose.

Author Contributions

Veronica Ravano: Conceptualization, Methodology, Software, Formal analysis, Investigation, Writing – Original draft preparation, Visualization; **Michaela Andelova:** Data curation, Investigation, Resources; **Mário João Fartaria**: Software, Data curation; **Mazen Fouad A-Wali Mahdi:** Software; **Reto Meuli**: Funding acquisition, Resources; **Bénédicte Maréchal:** Software, Data curation ; **Tomas Uher**: Data curation, Resources; **Jan Krasensky:** Data curation, Resources; **Manuela Vaneckova:** Data curation, Funding acquisition, Resources; **Dana Horakova:** Data curation, Funding acquisition, Resources; **Tobias Kober:** Conceptualization, Funding acquisition, Supervision; **Jonas Richiardi:** Conceptualization, Methodology, Investigation, Writing – Original draft preparation, Supervision, Project administration; **all:** Writing – Review and Editing

medRxiv preprint doi: https://doi.org/10.1101/2021.05.03.21256161; this version posted May 4, 2021. The copyright holder for this preprint
(which was not certified by peer review) is the author/funder, who has granted medRxiv a license to display the preprint in perpetuity.
It is made available under a CC-BY-NC 4.0 International license .

References

Aerts, H., Fias, W., Caeyenberghs, K., Marinazzo, D., 2016. Brain networks under attack: Robustness properties and the impact of lesions. Brain 139, 3063–3083. https://doi.org/10.1093/brain/aww194

Barkhof, F., 2002. The clinico-radiological paradox in multiple sclerosis revisited. Curr. Opin. Neurol. 15, 239–245. https://doi.org/10.1097/00019052-200206000-00003

Bassett, D.S., Sporns, O., 2017. Network neuroscience. Nat. Neurosci. 20, 353–364. https://doi.org/10.1038/nn.4502

Bates, E., Wilson, S.M., Saygin, A.P., Dick, F., Sereno, M.I., Knight, R.T., Dronker, N.F., 2003. Voxel-based lesion-symptom mapping. Nat. Neurosci. 6, 448–450. https://doi.org/10.1038/nn1050

Buckner, R.L., Krienen, F.M., Castellanos, A., Diaz, J.C., Yeo, B.T.T., 2011. The organization of the human cerebellum estimated by intrinsic functional connectivity. J Neurophysiol 106, 2322–2345. https://doi.org/10.1152/jn.00339.2011.

Bullmore, E.T., Bassett, D.S., 2011. Brain Graphs: Graphical Models of the Human Brain Connectome. Annu. Rev. Clin. Psychol. 7, 113–140. https://doi.org/10.1146/annurev-clinpsy-040510-143934

Bullmore, E.T., Sporns, O., 2009. Complex brain networks : graph theoretical analysis of structural and functional systems. Nat. Rev. Neurosci. 10, 186–198. https://doi.org/10.1038/nrn2575

Butzkueven, H., Chapman, J., Cristiano, E., Grand'Maison, F., Hoffmann, M., Izquierdo, G., Jolley, D., Kappos, L., Leist, T., Pöhlau, D., Rivera, V., Trojano, M., Verheul, F., Malkowski, J.P., 2006. MSBase: An international, online registry and platform for collaborative outcomes research in multiple sclerosis. Mult. Scler. 12, 769–774. https://doi.org/10.1177/1352458506070775

Calabrese, E., Badea, A., Coe, C.L., Lubach, G.R., Styner, M.A., Johnson, G.A., 2014. Investigating the tradeoffs between spatial resolution and diffusion sampling for brain mapping with diffusion tractography: Time well spent? Hum. Brain Mapp. 35, 5667–5685. https://doi.org/10.1002/hbm.22578

Carrera, E., Tononi, G., 2014. Diaschisis: Past, present, future. Brain 137, 2408–2422. https://doi.org/10.1093/brain/awu101

Catani, M., Dell'Acqua, F., Bizzi, A., Forkel, S.J., Williams, S.C., Simmons, A., Murphy, D.G., Thiebaut de Schotten, M., 2012. Beyond cortical localization in clinico-anatomical correlation. Cortex 48, 1262–1287. https://doi.org/10.1016/j.cortex.2012.07.001

Catani, M., Ffytche, D.H., 2005. The rises and falls of disconnection syndromes. Brain 128, 2224–2239. https://doi.org/10.1093/brain/awh622

Charil, A., Zijdenbos, A.P., Taylor, J., Boelman, C., Worsley, K.J., Evans, A.C., Dagher, A., 2003. Statistical mapping analysis of lesion location and neurological disability in multiple sclerosis : application to 452 patient data sets. Neuroimage 19, 532–544. https://doi.org/10.1016/S1053-8119(03)00117-4

Chow, L.S., Paramesran, R., 2016. Review of medical image quality assessment. Biomed. Signal Process. Control 27, 145–154. https://doi.org/10.1016/j.bspc.2016.02.006

Ciccarelli, O., Catani, M., Johansen-Berg, H., Clark, C., Thompson, A., 2008. Diffusion-based tractography in neurological disorders: concepts, applications,

medRxiv preprint doi: https://doi.org/10.1101/2021.05.03.21256161; this version posted May 4, 2021. The copyright holder for this preprint
(which was not certified by peer review) is the author/funder, who has granted medRxiv a license to display the preprint in perpetuity.
It is made available under a CC-BY-NC 4.0 International license .

and future developments. Lancet Neurol. 7, 715–727. https://doi.org/10.1016/S1474-4422(08)70163-7

Connors, J., Krzywinski, M., Schein, J., Gascoyne, R., Horsman, D., Jones, S.J., Marra, M.A., 2009. Circos : An information aesthetic for comparative genomics. Genome Res. 19, 1639–1645. https://doi.org/10.1101/gr.092759.109.19

De Vico Fallani, F., Richiardi, J., Chavez, M., Achard, S., 2014. Graph analysis of functional brain networks: Practical issues in translational neuroscience. Philos. Trans. R. Soc. B 369. https://doi.org/10.1098/rstb.2013.0521

Donahue, C.J., Sotiropoulos, S.N., Jbabdi, S., Hernandez-Fernandez, M., Behrens, T.E., Dyrby, T.B., Coalson, T., Kennedy, H., Knoblauch, K., Van Essen, D.C., Glasser, M.F., 2016. Using diffusion tractography to predict cortical connection strength and distance: A quantitative comparison with tracers in the monkey. J. Neurosci. 36, 6758–6770. https://doi.org/10.1523/JNEUROSCI.0493-16.2016

Dziedzic, T., Metz, I., Dallenga, T., König, F.B., Müller, S., Stadelmann, C., Brück, W., 2010. Wallerian degeneration: A major component of early axonal pathology in multiple sclerosis. Brain Pathol. 20, 976–985. https://doi.org/10.1111/j.1750-3639.2010.00401.x

Faivre, A., Robinet, E., Guye, M., Rousseau, C., Maarouf, A., Le Troter, A., Zaaraoui, W., Rico, A., Crespy, L., Soulier, E., Confort-Gouny, S., Pelletier, J., Achard, S., Ranjeva, J.P., Audoin, B., 2016. Depletion of brain functional connectivity enhancement leads to disability progression in multiple sclerosis: A longitudinal resting-state fMRI study. Mult. Scler. 22, 1695–1708. https://doi.org/10.1177/1352458516628657

Fan, L., Li, H., Zhuo, J., Zhang, Y., Wang, J., Chen, L., Yang, Z., Chu, C., Xie, S., Laird, A.R., Fox, P.T., Eickhoff, S.B., Yu, C., Jiang, T., 2016. The Human Brainnetome Atlas: A New Brain Atlas Based on Connectional Architecture. Cereb. Cortex 26, 3508–3526. https://doi.org/10.1093/cercor/bhw157

Fartaria, M.J., Bonnier, G., Roche, A., Kober, T., Meuli, R., Rotzinger, D., Frackowiak, R., Schluep, M., Du Pasquier, R., Thiran, J.P., Krueger, G., Bach Cuadra, M., Granziera, C., 2016. Automated detection of white matter and cortical lesions in early stages of multiple sclerosis. J. Magn. Reson. Imaging 43, 1445–1454. https://doi.org/10.1002/jmri.25095

Fartaria, M.J., Roche, A., Meuli, R., Granziera, C., Kober, T., Bach Cuadra, M., 2017. Segmentation of Cortical and Subcortical Multiple Sclerosis Lesions Based on Constrained Partial. MICCAI LCNS 10435, 516–524. https://doi.org/10.1007/978-3-319-66179-7

Fleischer, V., Radetz, A., Ciolac, D., Muthuraman, M., Gonzalez-escamilla, G., 2019. Graph Theoretical Framework of Brain Networks in Multiple Sclerosis : A Review of Concepts. Neuroscience 403, 35–53. https://doi.org/10.1016/j.neuroscience.2017.10.033

Foulon, C., Cerliani, L., Kinkingnéhun, S., Levy, R., Rosso, C., Urbanski, M., Volle, E., de Schotten, M.T., 2018. Advanced lesion symptom mapping analyses and implementation as BCBtoolkit. Gigascience 7, 1–17. https://doi.org/10.1093/gigascience/giy004

Fox, M., 2018. Mapping Symptoms to Brain Networks with the Human Connectome. N. Engl. J. Med. 379, 2237–2245. https://doi.org/10.1056/NEJMra1706158

Gorgoraptis, N., Wheeler-Kingshott, C.A.M., Jenkins, T.M., Altmann, D.R., Miller, D.H., Thompson, A.J., Ciccarelli, O., 2010. Combining tractography and cortical measures to test system-specific hypotheses in multiple sclerosis. Mult. Scler.

medRxiv preprint doi: https://doi.org/10.1101/2021.05.03.21256161; this version posted May 4, 2021. The copyright holder for this preprint
(which was not certified by peer review) is the author/funder, who has granted medRxiv a license to display the preprint in perpetuity.
It is made available under a CC-BY-NC 4.0 International license .

16, 555–565. https://doi.org/10.1177/1352458510362440
Griffis, J.C., Metcalf, N. V., Corbetta, M., Shulman, G.L., 2020. Lesion Quantification Toolkit: A MATLAB software tool for estimating grey matter damage and white matter disconnections in patients with focal brain lesions. bioRxiv 30, 102639. https://doi.org/10.1101/2020.07.28.225771
Grover, A., Leskovec, J., 2016. Node2vec: Scalable feature learning for networks. Proc. ACM SIGKDD Int. Conf. Knowl. Discov. Data Min. 13-17-Augu, 855–864. https://doi.org/10.1145/2939672.2939754
Hagberg, A.A., Schult, D.A., Swart, P.J., 2008. Exploring network structure, dynamics, and function using NetworkX. 7th Python Sci. Conf. (SciPy 2008) 11–15.
Hagmann, P., Cammoun, L., Gigandet, X., Meuli, R., Honey, C.J., Van Wedeen, J., Sporns, O., 2008. Mapping the structural core of human cerebral cortex. PLoS Biol. 6, 1479–1493. https://doi.org/10.1371/journal.pbio.0060159
Hamilton, W.L., Ying, R., Leskovec, J., 2017. Representation Learning on Graphs: Methods and Applications. Bull. IEEE Comput. Soc. Tech. Comm. Data Eng. 1–24.
Hayes, C.E., Ntambi, J.M., 2020. Multiple Sclerosis: Lipids, Lymphocytes, and Vitamin D. Immunometabolism 1–54. https://doi.org/10.20900/immunometab20200019
Horakova, D., Zivadinov, R., Weinstock-Guttman, B., Havrdova, E., Qu, J., Tamaño-Blanco, M., Badgett, D., Tyblova, M., Bergsland, N., Hussein, S., Willis, L., Krasensky, J., Vaneckova, M., Seidl, Z., Lelkova, P., Dwyer, M.G., Zhang, M., Yu, H., Duan, X., Kalincik, T., Ramanathan, M., 2013. Environmental Factors Associated with Disease Progression after the First Demyelinating Event: Results from the Multi-Center SET Study. PLoS One 8, 1–8. https://doi.org/10.1371/journal.pone.0053996
Jones, D.K., Knösche, T.R., Turner, R., 2013. White matter integrity, fiber count, and other fallacies: The do's and don'ts of diffusion MRI. Neuroimage 73, 239–254. https://doi.org/10.1016/j.neuroimage.2012.06.081
Klein, S., Staring, M., Murphy, K., Viergever, M. a., Pluim, J., 2010. elastix: A Toolbox for Intensity-Based Medical Image Registration. IEEE Trans. Med. Imaging 29, 196–205. https://doi.org/10.1109/TMI.2009.2035616
Kuceyeski, A.F., Vargas, W., Dayan, M., Monohan, E., Blackwell, C., Raj, A., Fujimoto, K., Gauthier, S.A., 2015. Modeling the relationship among gray matter atrophy, abnormalities in connecting white matter, and cognitive performance in early multiple sclerosis. Am. J. Neuroradiol. 36, 702–709. https://doi.org/10.3174/ajnr.A4165
Lin, X., Tench, C.R., Morgan, P.S., Niepel, G., Constantinescu, C.S., 2005. "Importance sampling" in MS: Use of diffusion tensor tractography to quantify pathology related to specific impairment. J. Neurol. Sci. 237, 13–19. https://doi.org/10.1016/j.jns.2005.04.019
Lipp, I., Parker, G.D., Tallantyre, E.C., Goodall, A., Grama, S., Patitucci, E., Heveron, P., Tomassini, V., Jones, D.K., 2020. Tractography in the presence of multiple sclerosis lesions. Neuroimage 209, 116471. https://doi.org/10.1016/j.neuroimage.2019.116471
Llufriu, S., Martinez-Heras, E., Solana, E., Sola-Valls, N., Sepulveda, M., Blanco, Y., Martinez-Lapiscina, E.H., Andorra, M., Villoslada, P., Prats-Galino, A., Saiz, A., 2017. Structural networks involved in attention and executive functions in

medRxiv preprint doi: https://doi.org/10.1101/2021.05.03.21256161; this version posted May 4, 2021. The copyright holder for this preprint
(which was not certified by peer review) is the author/funder, who has granted medRxiv a license to display the preprint in perpetuity.
It is made available under a CC-BY-NC 4.0 International license .

multiple sclerosis. NeuroImage Clin. 13, 288–296. https://doi.org/10.1016/j.nicl.2016.11.026

Lucchinetti, C., Brück, W., Parisi, J., Scheithauer, B., Rodriguez, M., Lassmann, H., 2000. Heterogeneity of multiple sclerosis lesions: Implications for the pathogenesis of demyelination. Ann. Neurol. 47, 707–717. https://doi.org/10.1002/1531-8249(200006)47:6<707::AID-ANA3>3.0.CO;2-Q

McInnes, L., Healy, J., Melville, J., 2018. UMAP: Uniform Manifold Approximation and Projection for Dimension Reduction. arXiv Prepr. arXiv1802.03426.

Muthuraman, M., Fleischer, V., Kolber, P., Luessi, F., Zipp, F., Groppa, S., 2016. Structural brain network characteristics can differentiate CIS from early RRMS. Front. Neurosci. 10, 1–12. https://doi.org/10.3389/fnins.2016.00014

Pawlitzki, M., Neumann, J., Kaufmann, J., Heidel, J., Stadler, E., Sweeney-Reed, C., Sailer, M., Schreiber, S., 2017. Loss of corticospinal tract integrity in early MS disease stages. Neurol. Neuroimmunol. NeuroInflammation 4. https://doi.org/10.1212/NXI.0000000000000399

Ravano, V., Andelova, Michaela Mahdi, M.F.A.-W., Meuli, R., Uher, T., Krasensky, J., Vaneckova, M., Horakova, D., Kober, T., Richiardi, J., 2019. Atlas-based tract damage mapping improves 4-year forecast of EDSS in multiple sclerosis, in: Multiple Sclerosis Journal, Vol. 25. pp. 182–183.

Ravano, V., Andelova, M., Fouad, M., Mahdi, A.-W., Meuli, R., Uher, T., Krasensky, J., Vaneckova, M., Horakova, D., Kober, T., Richiardi, J., 2020. Automated atlas-based mapping of white matter tract damage to multiple sclerosis symptoms, in: Proceedings of the International Society of Magnetic Resonance in Medicine. p. 1391.

Reich, D.S., Smith, S.A., Zackowski, K.M., Gordon-Lipkin, E.M., Jones, C.K., Farrell, J.A.D., Mori, S., van Zijl, P.C.M., Calabresi, P.A., 2007. Multiparametric magnetic resonance imaging analysis of the corticospinal tract in multiple sclerosis. Neuroimage 38, 271–279. https://doi.org/10.1016/j.neuroimage.2007.07.049

Richiardi, J., Achard, S., Bunke, H., Ville, D. Van De, 2013. Machine Learning with Brain Graphs. IEEE Signal Process. Mag. 30, 58–70. https://doi.org/10.1109/MSP.2012.2233865

Rocca, M.A., Amato, M.P., De Stefano, N., Enzinger, C., Geurts, J.J., Penner, I.K., Rovira, A., Sumowski, J.F., Valsasina, P., Filippi, M., 2015. Clinical and imaging assessment of cognitive dysfunction in multiple sclerosis. Lancet Neurol. 14, 302–317. https://doi.org/10.1016/S1474-4422(14)70250-9

Rocca, M.A., Valsasina, P., Meani, A., Falini, A., Comi, G., Filippi, M., 2016. Impaired functional integration in multiple sclerosis: a graph theory study. Brain Struct. Funct. 221, 115–131. https://doi.org/10.1007/s00429-014-0896-4

Schmitter, D., Roche, A., Maréchal, B., Ribes, D., Abdulkadir, A., Bach-Cuadra, M., Daducci, A., Granziera, C., Klöppel, S., Maeder, P., Meuli, R., Krueger, G., 2015. An evaluation of volume-based morphometry for prediction of mild cognitive impairment and Alzheimer's disease. NeuroImage Clin. 7, 7–17. https://doi.org/10.1016/j.nicl.2014.11.001

Shu, N., Duan, Y., Xia, M., Schoonheim, M.M., Huang, J., Ren, Z., Sun, Z., Ye, J., Dong, H., Shi, F.D., Barkhof, F., Li, K., Liu, Y., 2016. Disrupted topological organization of structural and functional brain connectomes in clinically isolated syndrome and multiple sclerosis. Sci. Rep. 6, 1–11. https://doi.org/10.1038/srep29383

medRxiv preprint doi: https://doi.org/10.1101/2021.05.03.21256161; this version posted May 4, 2021. The copyright holder for this preprint
(which was not certified by peer review) is the author/funder, who has granted medRxiv a license to display the preprint in perpetuity.
It is made available under a CC-BY-NC 4.0 International license .

Shu, N., Liu, Y., Li, K., Duan, Y., Wang, J., Yu, C., Dong, H., Ye, J., He, Y., 2011. Diffusion tensor tractography reveals disrupted topological efficiency in white matter structural networks in multiple sclerosis. Cereb. Cortex 21, 2565–2577. https://doi.org/10.1093/cercor/bhr039

Simioni, S., Amarù, F., Bonnier, G., Kober, T., Rotzinger, D., Du Pasquier, R., Schluep, M., Meuli, R., Sbarbati, A., Thiran, J.P., Krueger, G., Granziera, C., 2014. MP2RAGE provides new clinically-compatible correlates of mild cognitive deficits in relapsing-remitting multiple sclerosis. J. Neurol. 261, 1606–1613. https://doi.org/10.1007/s00415-014-7398-4

Solana, E., Martinez-Heras, E., Martinez-Lapiscina, E.H., Sepulveda, M., Sola-Valls, N., Bargalló, N., Berenguer, J., Blanco, Y., Andorra, M., Pulido-Valdeolivas, I., Zubizarreta, I., Saiz, A., Llufriu, S., 2018. Magnetic resonance markers of tissue damage related to connectivity disruption in multiple sclerosis. NeuroImage Clin. 20, 161–168. https://doi.org/10.1016/j.nicl.2018.07.012

Sporns, O., Tononi, G., Kötter, R., 2005. The human connectome: A structural description of the human brain. PLoS Comput. Biol. 1, 0245–0251. https://doi.org/10.1371/journal.pcbi.0010042

Telesford, Q.K., Joyce, K.E., Hayasaka, S., Burdette, J.H., Laurienti, P.J., 2011. The Ubiquity of Small-World Networks. Brain Connect. 1, 367–375. https://doi.org/10.1089/brain.2011.0038

Tievsky, A.L., Ptak, T., Farkas, J., 1999. Investigation of apparent diffusion coefficient and diffusion tensor anisotropy in acute and chronic multiple sclerosis lesions. Am. J. Neuroradiol. 20, 1491–1499.

Van Essen, D.., Ugurbil, K., Auerbach, E., Barch, D., Behrens, T.E.J., Bucholz, R., Chang, A., Chen, L., Corbetta, M., Curtiss, S.W., Della Penna, S., Feinberg, D., Glasser, M.F., Harel, N., Heathj, A.C., Larson-Prior, L., Marcus, D., Michalareas, G., Moeller, S., Oostenveld, R., Petersen, S.E., Prior, F., Schlaggar, B.L., Smith, S.M., Snyder, A.Z., Xu, J., Yacoub, E., Consortium, W.-M.H., 2012. The Human Connectome Project: A data acquisition perspective. Neuroimage 62, 2222–2231. https://doi.org/10.1115/JRC2014-3865

Vellinga, M.M., Geurts, J.J.G., Rostrup, E., Uitdehaag, B.M.J., Polman, C.H., Barkhof, F., Vrenken, H., 2009. Clinical correlations of brain lesion distribution in multiple sclerosis. J. Magn. Reson. Imaging 29, 768–773. https://doi.org/10.1002/jmri.21679

Watts, D.J., Strogatz, S.H., 1998. Small social network dynamic set. Science (80-.). 393, 440–442.

Yan, C., Gong, G., Wang, J., Wang, D., Liu, D., Zhu, C., Chen, Z.J., Evans, A., Zang, Y., He, Y., 2011. Sex- and brain size-related small-world structural cortical networks in young adults: A DTI tractography study. Cereb. Cortex 21, 449–458. https://doi.org/10.1093/cercor/bhq111

Yaou, L., Hao, W., Yunyun, D., Jing, H., Zhuoqiong, R., Jing, Y., Huiqing, D., Fudong, S., Kuncheng, L., Jinhui, W., 2017. Functional Brain Network Alterations in Clinically Isolated Syndrome and Multiple Sclerosis: A Graph-based Connectome Study. Radiology 282, 534–541. https://doi.org/10.1148/radiol.2016152843

Yeh, F.C., Panesar, S., Fernandes, D., Meola, A., Yoshino, M., Fernandez-Miranda, J.C., Vettel, J.M., Verstynen, T., 2018. Population-averaged atlas of the macroscale human structural connectome and its network topology. Neuroimage 178, 57–68. https://doi.org/10.1016/j.neuroimage.2018.05.027

medRxiv preprint doi: https://doi.org/10.1101/2021.05.03.21256161; this version posted May 4, 2021. The copyright holder for this preprint
(which was not certified by peer review) is the author/funder, who has granted medRxiv a license to display the preprint in perpetuity.
It is made available under a CC-BY-NC 4.0 International license .

Yeh, F.C., Tseng, W.Y.I., 2011. NTU-90: A high angular resolution brain atlas constructed by q-space diffeomorphic reconstruction. Neuroimage 58, 91–99. https://doi.org/10.1016/j.neuroimage.2011.06.021